AIP Advances

Tunable self-assembly of magnetotactic bacteria: Role of hydrodynamics and magnetism

Cite as: AIP Advances **10**, 015335 (2020); https://doi.org/10.1063/1.5129925
Submitted: 07 October 2019 . Accepted: 17 December 2019 . Published Online: 22 January 2020

Christopher J. Pierce, Hiran Wijesinghe, Emily Osborne, Eric Mumper, Brian Lower, Steven Lower, and Ratnasingham Sooryakumar

Tunable self-assembly of magnetotactic bacteria: Role of hydrodynamics and magnetism

Cite as: AIP Advances 10, 015335 (2020); doi: 10.1063/1.5129925
Presented: 7 November 2019 • Submitted: 7 October 2019 •
Accepted: 17 December 2019 • Published Online: 22 January 2020

Christopher J. Pierce,[1] Hiran Wijesinghe,[1] Emily Osborne,[1] Eric Mumper,[2] Brian Lower,[2] Steven Lower,[2,3,4] and Ratnasingham Sooryakumar[1,a)]

AFFILIATIONS

[1]Department of Physics, The Ohio State University, Columbus, Ohio 43210, USA
[2]School of Environment and Natural Resources, The Ohio State University, Columbus, Ohio 43210, USA
[3]School of Earth Sciences, The Ohio State University, Columbus, Ohio 43210, USA
[4]Department of Microbial Infection and Immunity, The Ohio State University, Columbus, Ohio 43210, USA

Note: This paper was presented at the 64th Annual Conference on Magnetism and Magnetic Materials.
[a)]sooryakumar.1@osu.edu

ABSTRACT

Self-assembly is an important process in biological systems and also a promising avenue toward dynamic and responsive micro- and nano-technologies. This study discusses the non-equilibrium self-assembly of inherently magnetic bacteria oriented perpendicular to a solid surface. An interplay between hydrodynamic and magnetic interactions leads to stable three-dimensional clusters in the long-time regime, which may be programmatically assembled, disassembled, and translated across a surface. The implications of the findings for the rational design of non-equilibrium self-assembly in general are discussed.

INTRODUCTION

Since Feynman's prescient lecture "There's Plenty of Room at the Bottom"[1] was first delivered, society has seen the development of Moore's law scaling in solid state electronic systems, the miniaturization of biology and chemistry experiments via microfluidic and lab-on-a-chip platforms, and the development of nanotechnology-based techniques that show potential to dramatically alter the future of medicine. These advancements extend the domain of machines over a cascade of hierarchical length scales into the micro- and nano-scale regimes. At the center of these developments is the problem of dynamically controlling matter at the sub-micron scale. Numerous approaches to this problem have been advanced, including optical methods such as photolithography[3] and optical tweezers,[4,5] direct micromanipulation through scanned probes,[6] magnetic particle manipulation,[7,8] Micro-electromechanical Systems (MEMS)[9] and several others. However, many of these methods suffer from limits imposed by their scalability and cost. Moreover, they lack some of the desirable properties of biological systems operating at comparable length scales, such as self-replication, healing and adaptation. This has motivated interest in alternative approaches to controlling matter that are derived from observations of such biological systems, which themselves maintain structure and function across length scales from the nanoscale to the organismal level and beyond. In many cases, biological systems achieve these ends through self-assembly, in which active components consume energy from environmental sources and achieve a structure and function through their cooperative interactions. This results in a high degree of precision, scalability and dynamic responsiveness in the structuring of microscopic matter. However, the exploitation of principles from nature for technological applications remains limited, in part because selecting the particular active components and their inherent interactions within the framework of self-assembly that will lead to a *desired* structure of interest, remains challenging. A better understanding of non-equilibrium self-assembly is needed to address this challenge. Conversely, such understanding could also provide insight into biological questions as well related, for example, to collective cell transport and cooperativity.

A typical example of non-equilibrium self-assembly is the group dynamics of both synthetic and biological microswimmers[10] that propel themselves through fluidic environments. The hydrodynamic wake produced by their propulsive activity leads to interactions with neighboring swimmers and nearby surfaces. These interactions in turn result in a variety of self-assembled patterns including bands,[11] vortices,[12,13] pearling structures,[14] and two-dimensional (2D) clusters near a boundary.[15–18] Hydrodynamic clustering near surfaces has been observed in several microorganisms ranging in size from 100s of μm in the case of the algae *Volvox*[15] to several different bacterial species[17,16,19,18] ranging from 1-10 μm. In many of these systems an external force causes the primary component of the organism's propulsive force to be oriented perpendicular to a solid-liquid or air-liquid interface resulting in a flow perpendicular to the boundary. As the propulsive mechanism of the cell continually drives the organism into the boundary, fluid is expelled away from the surface, which is then circulated back downward, causing near-surface contractile flows that draw nearby cells toward one another. The resulting flow pattern is well described by that of a stokeslet[15,20,19] (a point force acting on the fluid) and the appropriate image system (which accounts for the presence of the surface).

In the majority of examples of this form of clustering, the orientation responsible for the contractile flow arises spontaneously under environmental conditions. For instance, in the algae *Volvox*, gravitational effects are responsible for the orientation, while in the fast swimming bacterium *Thiovulum majus*,[16,18] the orientation is hydrodynamic in origin. However, in the case of magnetic bacteria, the perpendicular configuration does not arise spontaneously but instead can be imposed through the application of a weak magnetic field perpendicular to the surface. The tunability of this external field allows the interactions to be programmatically removed and restored, allowing a systematic study of the kinetics of cluster formation. This has revealed that the cluster size scales logarithmically in time, which is conjectured to arise from a combination of the finite range of the hydrodynamic interactions, as well as the presence of magnetic dipole-dipole repulsion.[19]

In this article, the dynamics of these clusters are explored over extended time intervals (for periods of ~20 minutes). It is found that after an initial logarithmic cluster growth phase, the self-assembled objects approach a quasi-static state (in the long-time limit) that is maintained far from equilibrium. In addition, their behavior is probed beyond the surface confining the bacteria, revealing the 3D structure of the clusters, which are found to extend outward from the surface plane. These self-assembled columnar structures appear to display an overall quasi-stokeslet dominant flow field, drawing cells inward near the confining surface, propelling them upward through a column of cells in the structure, and expelling them near the top of the structure under the influence of convective flows, much like the flow describing an individual cell oriented at the surface.

Furthermore, as a consequence of the magnetic field-based control of the oriented bacteria, the resulting self-assembled objects may be directly manipulated – tunably assembled/re-assembled, and transported linearly across a surface. While this system has implications for questions of biological and engineered self-assembly in general, it may also be of direct use in applications where a biocompatible microscopic agent is required to perform tasks, such as manipulating and transporting cargo. By employing inherently magnetic strains of bacteria, this system bridges the gap between engineered and living systems. While the swimmers are biological in nature, they are readily integrated into magnetic field based control systems. In this way, studies of their dynamics contribute to biomimetic engineering approaches through the application of the discerned principles that govern their motion. However, because of their simple integration with existing electronic devices via magnetic control, they may be directly exploited for technological aims as well.[2,21]

METHODS

Magnetotspirillum magneticum AMB-1[22] is an inherently magnetic swimming bacterium of the magnetotactic bacteria group. It derives its magnetic properties from chains of membrane-bound magnetite (Fe_3O_4) nanoparticles called magnetosomes,[23] which are rigidly embedded within the cell body and constrained to lie nearly parallel to (within 20° of[24]) the cell's swimming axis (See TEM image in Fig. 1, a, b). These nanocrystals occur over a narrow range of sizes with a mean size of~50 nm and are found to be in the single domain magnetic state.[23] As evident in the TEM image of Fig. 1b, the mature magnetite crystal size in AMB-1 is about 50 nm, placing them in the stable single magnetic domain size range. This is significant, in that these nanocrystals are magnetic at ambient temperature without having to be placed in an external magnetic field. Much smaller sized particles that are superparamagnetic, do not have a stable, remanent magnetization at ambient temperature. Cells initially produce these smaller particles, which eventually

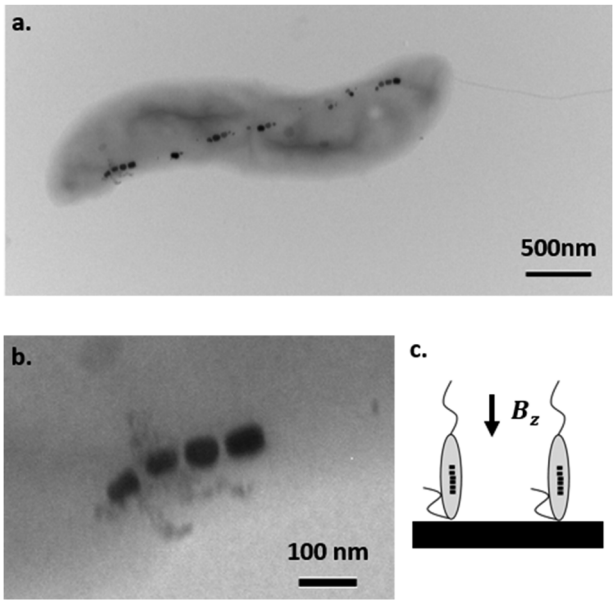

FIG. 1. a) TEM image showing *M. magnetic* AMB-1. b) magnified image of magnetosome chain fragment. c) schematic illustration of AMB-1 alignment parallel to an external field B_z orienting the cell perpendicular to the surface.

grow into mature single domain sized crystals. In much larger crystals (> 150 nm for example), domain walls tend to occur, causing these crystals to be non-uniformly magnetized, thereby reducing the remanent magnetization. The absence of these larger particles in the cell body reflects the increased energy, and reduced magnetic advantage of the multi domain particles relative to those in a single domain state. Because these single-domain nanocrystals are arranged linearly in a chain, they provide the cell with a fixed magnetic moment. AMB-1 possesses two flagella at either end of the body. By selectively powering the rear or forward flagellum, the cell may swim parallel or anti-parallel to magnetic field lines,[25] allowing external control over their orientation and swimming direction relative to a surface. These properties of AMB-1, together with the ability to magnetically orient the cell swimming direction near a surface as illustrated schematically in Fig. 1c, make it a valuable model organism for studying hydrodynamically mediated collective behavior.

Magnetic fields are applied to AMB-1 under microscope observation using a previously described system.[26] AMB-1 cells are cultured in serum bottles on Magnetic *Spirillum* growth media (MSGM 1653 from the American Type Culture Collection with Frankel's vitamin solution and modified Wolfe's mineral solution[27]). Bacteria samples are withdrawn via a syringe into micro-centrifuge tubes. Samples are then either directly pipetted into the device (providing low density samples) or centrifuged to create a high density pellet which is then pipetted into the system (providing high density samples). The samples are contained in a slab of fluid using a double-sided tape or Polydimethylsiloxane PDMS o-ring (with heights ranging from ~100-500μm) and two coverslips and then imaged under conventional bright field microscopy while being subjected to the magnetic field arising from a tunable 3-axis electromagnet.[26] From an initially random position, cells are made to orient perpendicular to a surface by applying a field perpendicular to the glass coverslips (B_z). Once the cells are in such an orientation, they begin to interact coherently, and the clustering process begins immediately.

RESULTS

Figure 2 illustrates the clustering process of a low density AMB-1 suspension. An initially disordered group of cells is oriented perpendicular to the lower coverslip surface by a field B_z and begins to interact through mutually attractive flow fields. After ~30 s, several clusters are formed, as illustrated in the lower panel. To confirm that such clustering can arise from a combination of hydrodynamic and magnetic interactions a 2D stochastic differential equation was constructed containing the following interaction terms: 1) a hydrodynamic model of the stokeslet flow based interaction from previous work,[15,19,20] 2) magnetic dipole-dipole interactions, 3) a stochastic force, and 4) hard sphere repulsion to prevent cell overlap. This equation was then numerically integrated for N=400 cells in a 350 by 350 um square domain with periodic boundary conditions. Figure 3 shows simulation results beginning with a random cell distribution at t=0 (upper panel) evolving into clusters (lower panel) shown at t=300s. Hence the underlying magnetic and hydrodynamic interactions are found to reproduce the basic clustering phenomenon observed in the experiment.

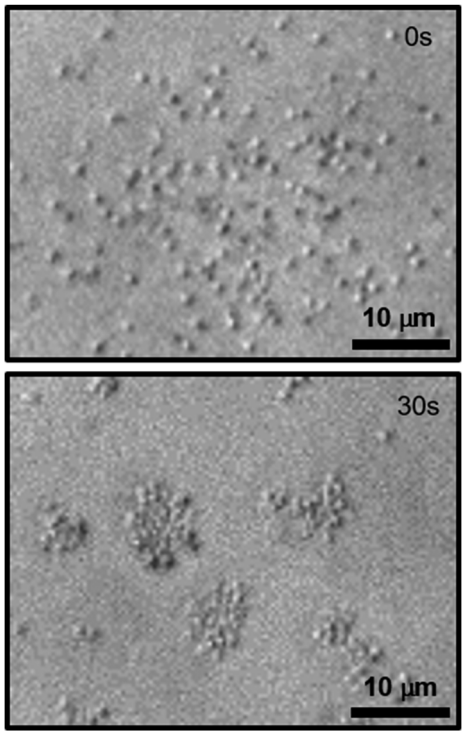

FIG. 2. An initially disordered set of perpendicularly oriented cells (top panel) evolves into clusters (bottom panel) over time.

Figure 4 shows the long time clustering behavior of a higher density sample. Figure 4a (Multimedia view) shows images of the clustering process for 900s after the initially disordered cells were subjected to a perpendicular field (B_z=100 G). Initially, the cells form a growing network of elongated regions of high cell density (5s, 25s). Over time, shearing forces from rotlet flow fields that arise from cell body rotation[19] break these linear objects apart. The objects then coalesce into generally circular objects which persist for the remaining duration of the experiment (250-900s). Figure 4b shows a detailed view of the coalescence of several objects into circular objects under attractive and rotating fields.

To quantify the growth of the clusters, the radial distribution function G(r) (Fig. 4c) is computed from micrcoscopy images and changes to its shape over time are observed. G(r) gives the probability distribution of cell-cell distances relative to the expectation for an ideal gas (equiprobability). Figure 3d shows G(r) for a range of times, with each curve displaced for clarity. When the G(r) curve drops below the equiprobability curve (horizontal line), that indicates a reduced probability of finding cells at the corresponding distance r. Alternatively, when the curve passes above the line, the probability of finding objects separated by that distance is enhanced. At low r (< 5μm), an initial peak is found whose area is proportional to the number of cells within clusters (see Fig 3c). At increasing r, a crossing of the equipotential line corresponds with the largest cluster radius r$*$ in the image (labeled

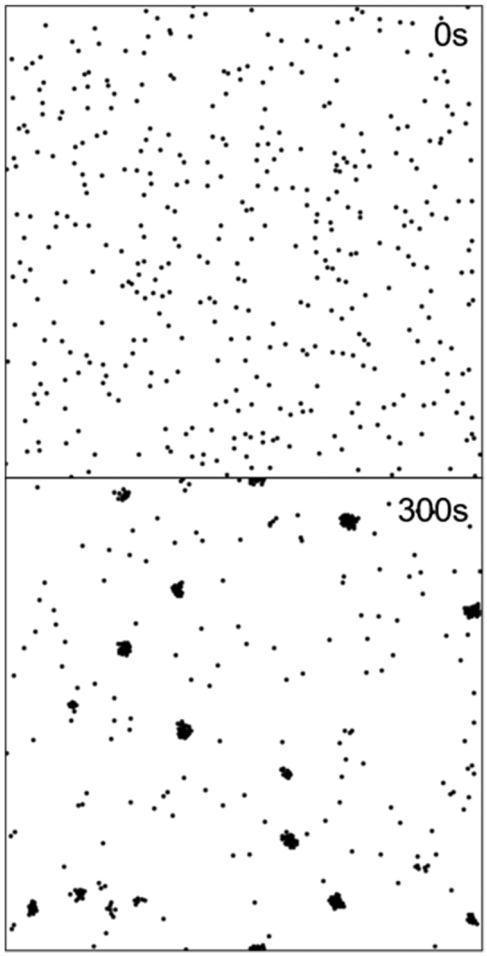

FIG. 3. Simuations results of an initially random cell distribution of 400 cells at t=0 (upper image) and at t=300s (lower image) in a 350μm sized box.

as black circles in Fig 3d). As time progresses, the crossing occurs at larger r corresponding to an increasing cluster size. In the early time regime, r∗ increases rapidly along with pronounced changes to the shape of G(r) (blue curves). The peaks at larger r correspond with the mean cluster-cluster distance. As time progresses, the peaks broaden as the line-crossing moves outward. However, after roughly 250 seconds, the shape of the curve ceases to change qualitatively, and the cluster size remains approximately fixed, fluctuating around a mean radius of 50 μm. In this regime the clusters cease to change appreciably and remain largely circular, as magnetic repulsion between the cells begins to limit the ability of the clusters to accumulate new cells.

The mean cluster size (r∗) inferred from the G(r) curves is plotted against time in Fig. 4e. This reveals that after an initial transient period (in this particular sample, lasting ~10s), the clusters proceed to scale logarithmically until ~250 seconds, after which point the average cluster size remains quasi-static and fluctuates. These fluctuations of r∗ are quite pronounced, reflecting the small number of clusters within the frame of observation and the exit and entrance of objects from the frame as a result of a weak background flow.

To further characterize the time evolution of the clusters, the number of cluster merging events is estimated as a function of time. This is accomplished by first binarizing the recorded microscopy images. An erosion-dilation process step is performed on the image to remove small objects, and the number of objects is counted as a function of time. By noting the drop in the total number of objects from the initial frame after application of the field, the net number of cluster merge events at a given time is calculated (total merge events minus total splitting events), as shown in Figure 3f. After an initially rapid increase in the total number of merge events (see Fig. 4f inset) the *rate* drops dramatically and the net number of merge events saturates. It is worth noting that from 250s onward, only 2 individual large scale merge events (involving clusters larger than ~20 μm) are observed (see See Fig 4a, Multimedia view). A fluctuating background of merge/division events arises from the smaller objects joining and separating from these larger objects without resulting in large changes to the total number of objects in the field of view.

Additionally, the time scale at which the cumulative number of merge events reaches saturation (~50s) is not commensurate with the time scale at which the clusters reach maximum size and cease to grow (250s). This suggests that in the intervening time period the clusters largely re-arrange themselves, rather than increasing their characteristic size through accretion of cells. This is further corroborated by studying the circularity (C) of the clusters as a function of time (Fig. 4g), which is calculated by numerically determining each object's perimeter l and area A from the binarized images and calculated via $C = 4\pi\left(\frac{A}{l^2}\right)$. Initially, small clusters form, which are generally circular in shape. This then gives rise to less circular elongated network-like structures (see Fig. 4a Multimedia view, at 5s and 25s), leading to a drop in the circularity. Thereafter, as the networks begin to break up and give rise to larger isolated islands, the clusters attain their final, largely circular form and remain stable throughout the duration of the quasi-static regime.

The 3D extent of the clusters was imaged using a motorized objective mount to move the imaging plane from the surface into the bulk fluid at known heights. Fig 4a shows a low density sample of clusters assembled for ~15 minutes under a B_z=100 Oe field. The panel on the top left shows an image of the clusters at the confining surface while the right panel depicts the corresponding cluster at a height of roughly 70 μm. The reduced density of the cluster at this greater distance from the surface suggests that the clusters taper as they grow vertically larger. It is observed that clusters of a larger area are able to persist to greater heights with relatively constant areal density.

In image planes near the confining surface the flows are contractile while at greater distances from the surface, the flow becomes extensile, propelling cells away from the cluster. Fig. 5 show a large cluster from a higher density sample at a height of ~150 μm (Fig. 5b Multimedia view) and ~350 μm (Fig. 5c Multimedia view). Particle Image Velocitmetry (PIV) is used to estimate the flow of cells outside the cluster, revealing a net flux of cells into the cluster at the lower surface (Fig. 5b Multimedia view), and a net outward flux at the higher surface (Fig. 5c, Multimedia view).

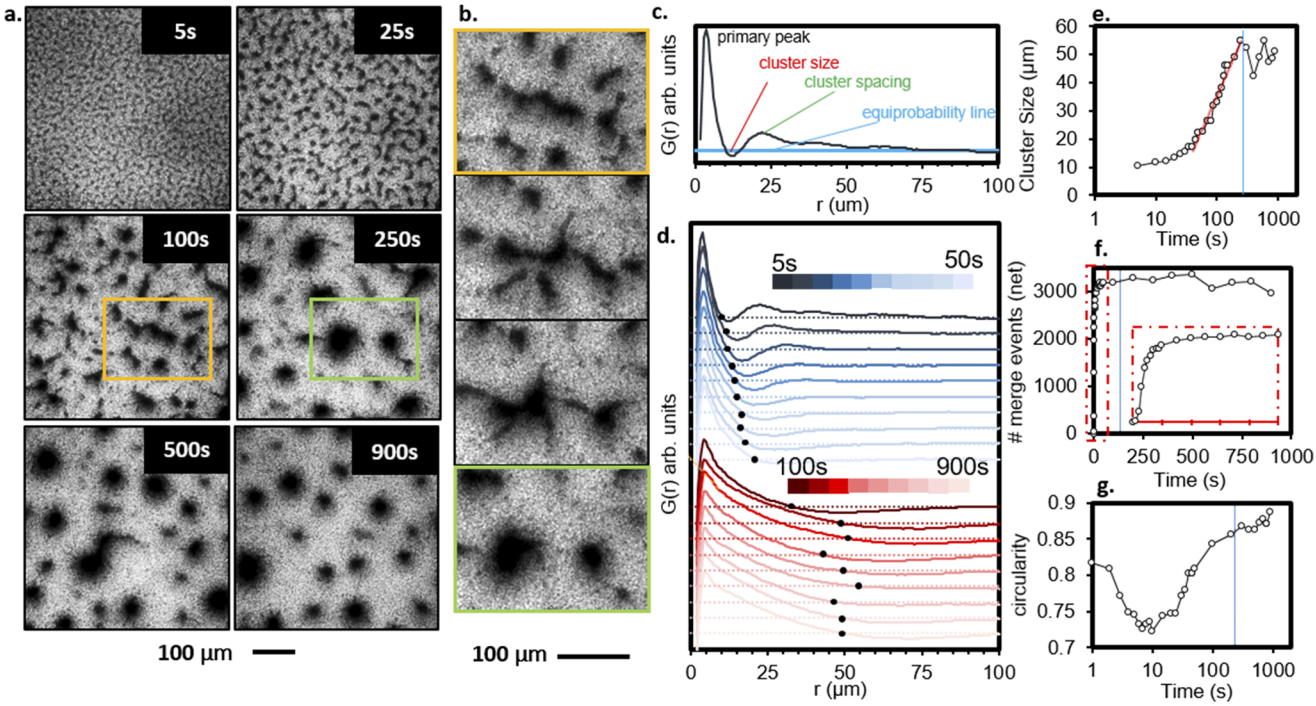

FIG. 4. a, sequence of images illustrating the transition from extensive network structures (5-25s) give rise to irregular objects (100s) which coalesce into stable circular objects (2Figure0-900s). b) Detail showing the formation of a single circular cluster from multiple irregular objects. c) Typical G(r) curve illustrating the primary peak associated with cells within the clusters, the crossing of G(r) with the equiprobability line corresponding with cluster size, and the peak associated with cluster-cluster spacing. d) G(r) over time in the initial fast growing regime (5-50s, in steps of 5s) shown in blue and in the quasi-static, long-time limit, shown in red (100-900s in steps of 100s). Black circles illustrate the maximum cluster size at each time step. e) cluster size versus time showing transient, logarithmic and quasi-static phases of growth. f) Merge events over time showing inset detail of initial rapid growth. g) Mean circularity of the clusters vs. time. In e, f, and g, the blue vertical lines show the onset of the quasi-static phase. Multimedia view: a: https://doi.org/10.1063/1.5129925.1

The 3D extension of the clusters and the transition from contractile to repellant flow can be understood by considering the stokeslet flow fields of the individual cells. These asymetric flow fields produce the contractile flows near the surface that lead to the initial near-surface cell clustering. However, as the clusters grow denser, fluid moving away from the surface, propelled by flagellar activity, pushes cells within the cluster away from the surface, leading to the extension of the cluster into the bulk. As the clusters accumulate cells, the net perpendicular flow in the center of the cluster increases, driving the vertical extension further.

Because of the linear fluid mechanics at low Reynold's number,[28] the flow from multiple cells is merely additive, and hence the net flow from a column of stokeslet swimmers pressing into a surface is expected to display a similar geometry to the flow field of individual cells. As with individual cells, near the surface, a large contractile flow pulls cells into the cluster. When the fluid pushed away from the surface recirculates back down to the surface, in a convective flow, cells in the upper planes of the cluster are pushed away and back down to the surface. Similarly, these largely columnar 3D micro-objects should behave in the far field as super-organismal magnetic dipoles. It has been previously conjectured[19] that the finite cut-off of the hydrodynamic interactions due to stochastic and other effects, and the persistence of magnetic dipolar repulsion for long distances is responsible for the self-limiting behavior evident in the cluster assembly process. It is speculated that the upward flux of cells near the center of the column may place additional constraints on the overall lateral extent. A cluster of unlimited lateral size is likely to be unstable due to the accumulation of flow in its interior directed away from the surface. Furthermore, the role that the repellant flows (see green arrows in Fig. 5) specifically play in the 3D dynamics of merging events as yet remains unclear.

Having identified the existence of quasi-stable self-assembly in the long time regime. the manipulation of such clusters with in-plane fields, and related possible applications is considered. In order to manipulate the cluster shapes, clusters were first produced at various densities under purely orthogonal fields and allowed to develop into the quasi-static regime (> 15 minutes). The clusters were then observed with the addition of in-plane fields. Under weak fields (B_x<10 *Oe*), the cell clusters translate across the surface in the direction close to the orientation of the in-plane field, remaining mostly intact. Clusters may be translated at a constant angle to the in-plane field, as well as relative to each other (Fig. 6a), an effect arising from the lateral movement of tilted cells near surfaces.[29] As the cells are oriented further into the planar direction by larger in-plane fields (~50 Oe) the clusters begin to distort themselves in the direction of

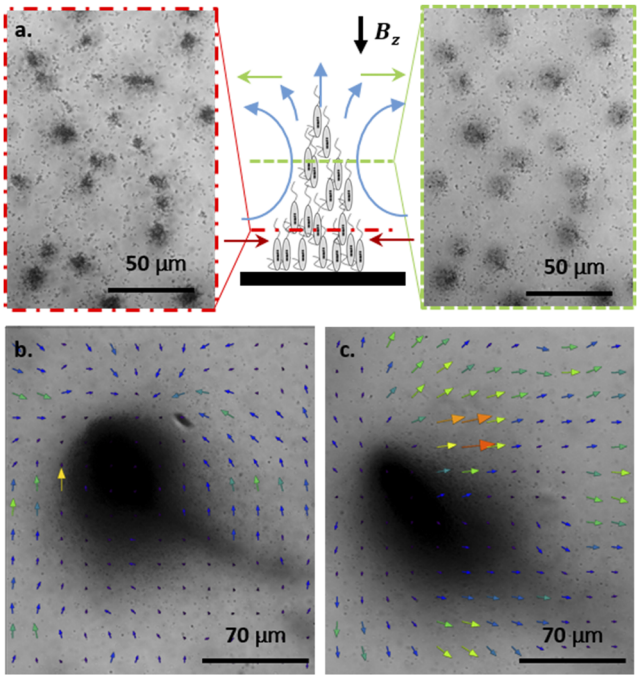

FIG. 5. a) A cluster imaged at the surface (left) and ~70 microns above (right) along with schematic illustration of 3D tapered structure showing regions of contractile cell accumulation (Red arrows) and dispersal (green arrows) as well as the geometry of the convective flow (blue arrows). b) A large cluster imaged at a height of 150 and c) 350 μm along with PIV flow field (color indicates vector magnitude) revealing a net accumulation of cells in lower regions and a net expulsion of cells in the upper portions of the column. Multimedia views: b: https://doi.org/10.1063/1.5129925.2; c: https://doi.org/10.1063/1.5129925.3

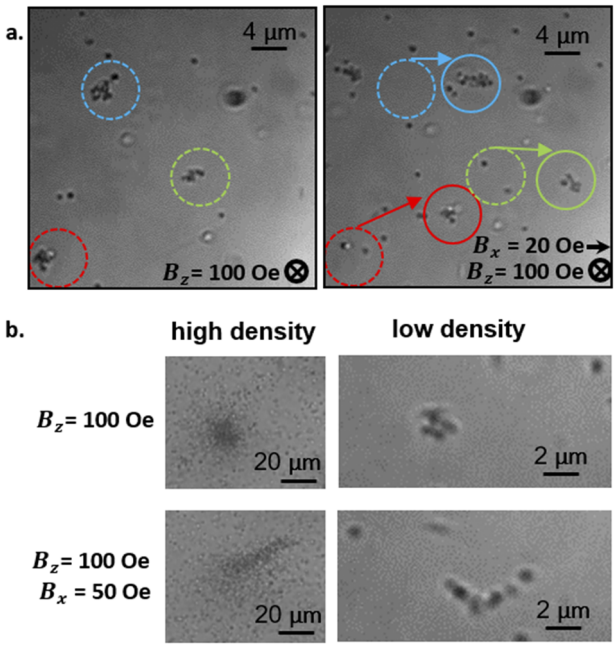

FIG. 6. a) initial cluster positions (left, dashed circle) and translated clusters (right, solid circles) after application of an inplane field for ~10s. b) A larger in-plane field (50 Oe) results in shearing and ultimately disassembly of the clusters in a high density case (left) and a lower density sample (right) over an interval of ~1.5 seconds.

the B_x field until they are dissolved entirely into individual cells. This disbanding arises from several effects: 1) as the clusters are tilted, the cells achieve a velocity in the x-direction; because the cells' velocities are widely distributed, those moving at different speeds start to separate, 2) as noted above, tilted AMB-1 cells are known to swim in non-parallel paths,[29] further expanding the cluster footprint, and 3) the attractive hydrodynamic components are reduced as the cells deviate from an orientation normal to the surface. As seen in Fig. 6b higher density clusters can persist for longer times under inplane fields relative to low density cases with smaller total hydrodynamic attraction. This ability to distort the geometry of the clusters into linear objects or to translate the clusters across surfaces may prove valuable in micro-manipulation. Translating clusters may be capable of applying considerable forces to suspended micro-objects in order to manipulate them. For instance clusters could be used to transport cargo to targeted locations and then disassembled, allowing the transported object to remain at its final destination. This approach could be further enhanced by exploiting micromagnetic structures to confine and contollably release the clusters from targeted locations, analogous to previous studies on individual cells.[30] Subsequent reassembly of the clusters could then be used to sequentially manipulate multiple objects, leading to a flexible micro-manipulation and assembly platform powered by the MTB.

CONCLUSION

In summary, it has been shown that in the long-time limit, hydrodynamically self-assembled magnetic bacteria oriented perpendicular to a surface are self-limiting, reaching a quasi-static state and hence provides an active analog to the so-called "self-focusing regime"[31] in inactive colloidal systems. This suggests a model for the design of self-assembled systems more generally – competing interactions with differing length-scales can lead to consistent stable structure formation in designed artificial systems. As the clusters expand, a transition from an initial network-like structure is found to give rise to circular objects which persist for extended periods of time. Additionally, as the clusters grow laterally across the surface, they begin to extend away from the surface and into the bulk fluid under the influence of convective flows. These 3D columnar objects are self-similar to the individual component cells – they display large scale flows which are generally consistent with those of a stokeslet and its image system and behave as macroscopic magnetic dipoles. Unlike the individual cells, these macroscopic magnetic dipoles no-longer coalesce. It is conjectured that the rescaling process is halted when the hydrodynamic and magnetic interactions become comparable, although the role of extensile flows in the upper regions of the columns may additionally inhibit late-time merge events. Finally, it was demonstrated that clusters may be directed along controlled paths or distorted under the influence of in-plane fields, and may be controllably assembled/disassembled. This ability suggests that clusters of AMB-1 could serve as a system for manipulating microscopic objects in lab-on-a-chip devices. In this sense, AMB-1 can serve not

only as a model for self-assembly processes in general technological endeavors, but may themselves be a promising candidate for direct use in engineered systems – acting as a self-organized microscopic agent.

ACKNOWLEDGMENTS

This material is based upon work supported by the National Science Foundation under Grants No. ECCS 1710598 and EAR-1424138. We also thank Hallie Georskey and Mr. Jeremy Rummer from Grandview Heights High School, as well as Rhea Mehta for assistance with cell culturing.

REFERENCES

[1] R. P. Feynman, Eng. Sci. **23**, 22–36 (1959).
[2] O. Felfoul, M. Mohammadi, S. Taherkani, D. de Lanauze, Y. Xu, D. Loghin, S. Essa, S. Jancik, D. Houle, M. Lafleur, L. Gaboury, M. Tabrizian, N. Kauo, M. Atkin, T. Vuoung, G. Batists, N. Beuchemin, D. Radzioch, and S. Martel, Nat. Nanotechnol. **11**, 941 (2016).
[3] J. T. M. Stevenson and A. M. Gundlach, J. Phys. E: Sci. Instrum. **19**, 654 (1986).
[4] A. Ashkin, J. M. Dziedzic, J. E. Bjorkholm, and S. Chu, Opt. Lett. **11**, 288–290 (1986).
[5] D. Gao, W. Ding, M. Nieto-Vesperinas, X. Ding, M. Zhang, C. T. Lim, and C.-W. Qiu, Light: Science & Applications **6**, e17039 (2017).
[6] R. D. Piner, J. Zhu, F. Xu, S. Hong, and C. A. Mirkin, Science **283**, 661–663 (1999).
[7] S. Lauback, K. R. Mattioli, A. E. Marras, M. Armstrong, T. P. Rudibaugh, R. Sooryakumar, and C. E. Castro, Nat. Comm. **9**, 1446 (2018).
[8] K. Gunnarsson, P. Roy, S. Felton, J. Pihl, P. Svedlindh, S. Berner, H. Lidbaum, and S. Oscarsson, Adv. Mater. **17**, 1730–1734 (2005).
[9] H. H. Gatzen, V. Saile, and J. Leuthold, "Introduction—MEMS, a historical perspective," in *Micro and Nano Fabrication* (Springer, Berlin, Heidelberg, 2015).
[10] E. Lauga and T. R. Powers, Rep. Prog. Phys. **72**, 096601 (2009).
[11] X. Fu, S. Kato, J. Long, H. H. Mattingly, C. He, D. C. Vural, S. W. Zucker, and T. Emonet, Nat. Comm. **9**, 2177 (2018).
[12] D. Nishiguchi, I. S. Aranson, A. Snezhko, and A. Sokolov, Nat. Comm. **9**, 4486 (2018).
[13] H. Wioland, F. G. Woodhouse, J. Dunkel, and R. E. Goldstein, Nature Physics **12**, 341–345 (2016).
[14] N. Waisbord, C. T. Lefèvre, L. Bocquet, C. Ybert, and C. Cottin-Bizonne, Phys. Rev. Fluids **1**, 053203 (2016).
[15] K. Drescher, K. C. Leptos, I. Tuval, T. Ishikawa, T. J. Pedley, and R. E. Goldstein, Phys. Rev. Lett. **102**, 168101 (2009).
[16] A. P. Petroff, X.-L. Wu, and A. Libchaber, Phys. Rev. Lett. **114**, 158102 (2015).
[17] X. Chen, X. Yang, M. Yang, and H. P. Zhang, Europhys. Lett. **111**, 54002 (2015).
[18] A. P. Petroff and A. Libchaber, New J. Phys. **20**, 015007 (2018).
[19] C. J. Pierce, H. Wijesinghe, E. Mumper, B. H. Lower, S. K. Lower, and K. Sooryakumar, Phys. Rev. Lett. **121**, 188001 (2018).
[20] T. Squires, J. Fluid Mech. **443**, 403 (2001).
[21] S. Martel, C. Tremblay, S. Ngakeng, and G. Langlois, Appl. Phys. Lett. **89**, 233904 (2006).
[22] C. Lefevre and D. Bazylinski, Microbiol. Mol. Biol. Rev. **77**, 497 (2013).
[23] D. Bazylinski and R. Frankel, Nat. Rev. Microbiol. **2**, 217 (2004).
[24] L. L. Nagard, L. Yu, M. Rajkotwala, S. Barkley, D. A. Bazylinski, A. P. Hitchcock, and C. Fradin, Physical Biology **16**, 066008 (2018).
[25] D. Murat, M. Herisse, L. Espinosa, A. Bossa, F. Alberto, and L. Wu, J. Bacteriol. **197**, 3275 (2015).
[26] G. Vieira, T. Henighan, A. Chen, A. J. Hauser, F. Y. Yang, J. J. Chalmers, and R. Sooryakumar, Phys. Rev. Lett. **103**, 128101 (2009).
[27] R. B. Frankel, D. A. Bazylinski, and B. L. Taylor, Biophys. J **73**, 994–1000 (1997).
[28] E. Purcell, Am. J. Phys. **45**, 3 (1977).
[29] C. J. Pierce, E. Mumper, E. E. Brown, J. T. Brangham, B. H. Lower, S. K. Lower, F. Y. Yang, and R. Sooryakumar, Phys. Rev. E **95**, 062612 (2017).
[30] C. J. Pierce, E. Osborne, E. Mumper, B. H. Lower, S. K. Lower, and R. Sooryakumar, Biophys. J. **117**, 1250–1257 (2019).
[31] S. M. Dammer and D. E. Wolf, Phys. Rev. Lett. **93**, 150602 (2004).